Journal of Materials Chemistry C

Accepted Manuscript

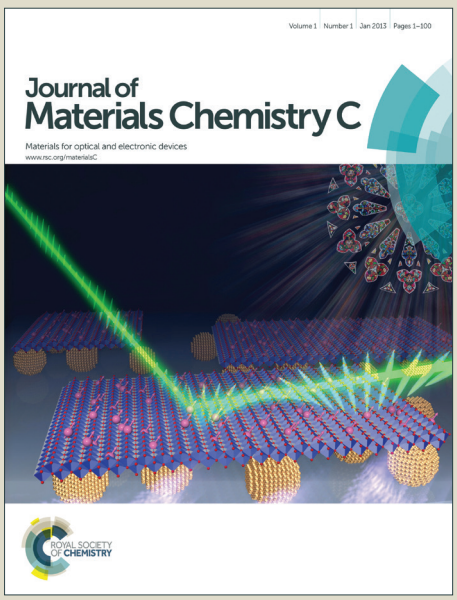

ROYAL SOCIETY OF CHEMISTRY

www.rsc.org/materialsC

Cite this: DOI: 10.1039/c0xx00000x

www.rsc.org/xxxxxx

ARTICLE TYPE

Synthesis of ultra-small $BaLuF_5$: Yb^{3+}, Er^{3+}@ $BaLuF_5$: Yb^{3+} active-core-active-shell nanoparticles with enhanced up-conversion and down-conversion luminescence by a layer-by-layer strategy

Yongling Zhang[a], Xiaohui Liu[a], Yanbo Lang[a], Zhen Yuan[b], Dan Zhao[a*], Guanshi Qin[a*], Weiping Qin[a*]

Received (in XXX, XXX) Xth XXXXXXXXX 20XX, Accepted Xth XXXXXXXXX 20XX
DOI: 10.1039/b000000x

Ultra-small luminescent nanoparticles (NPs) are quite desirable for optoelectronic and biomedical applications. However, it is still a challenge to synthesize ultra-small NPs with high brightness owing to non-radiative energy losses caused by the surface defects as well as from vibrational deactivation ascribed to solvent molecules and ligands absorbed on the NPs. In this paper, we reported a strategy to improve up- and down-conversion luminescence of ultra-small $BaLuF_5$: Yb^{3+}, Er^{3+} NPs by using multi-layer active-shells (containing Yb^{3+}). Sub-10 nm $BaLuF_5$: Yb^{3+}, Er^{3+}@ (X-shell, X=1~5) $BaLuF_5$: Yb^{3+} NPs were synthesized via a high boiling solvent process through a layer-by-layer strategy. Up- and down-conversion fluorescence spectra of the NPs were recorded and analyzed by using a 980 nm laser diode as the excitation source. In comparison with optical properties of $BaLuF_5$: Yb^{3+}, Er^{3+} NPs, the intensities of up- (~545 nm) and down-conversion (~1530 nm) fluorescence were enhanced by 52 and 9.8 times after coating 5-layer active-shells ($BaLuF_5$: Yb^{3+}) on the $BaLuF_5$: Yb^{3+}, Er^{3+} NPs, respectively. In addition, the intensities of up- and down-conversion fluorescence of the $BaLuF_5$: Yb^{3+}, Er^{3+} NPs with multi-layer active-shells were 1.3 and 1.1 times larger than those of the $BaLuF_5$: Yb^{3+}, Er^{3+} NPs with one thick-layer active shell, respectively. These results showed that multi-layer active-shells could be used to not only suppress surface quenching but also transfer the pump light to the core region efficiently through Yb^{3+} ions inside the active-shells.

1 Introduction

Lanthanide-doped up-conversion (UC) and down-conversion (DC) nanoparticles (NPs) have found numerous applications in many fields, such as solar cells, optical waveguide amplifiers, three-dimensional displays, photo-catalysis, and biomedicine (e.g., bio-labels, bio-imaging and photodynamic therapy (PDT)).[1-19] Especially, ultra-small (<10 nm) UCNPs are quite desirable for optical waveguide amplification and biomedical applications since they exhibit a good dispersibility in various solvents.[20,21,40] However, the luminescence quantum yield of ultra-small NPs is generally low due to nonradiative energy losses caused by the surface defects as well as from vibrational deactivation ascribed to solvent molecules and ligands absorbed on the NPs. To overcome this deficiency, various strategies have been developed to improve the luminescence of ultra-small NPs. One effective strategy is the construction of core-shell architectures, where an inert shell is grown around the luminescent core with similar lattice constants and can preclude surface defects from interacting with lanthanide ions.[22-31] $NaYF_4$: Yb, Er@ $NaYF_4$ nanoparticles were synthesized by Ren et al., the intensity of UC emission of the core-shell nanoparticles was as much as 16 times brighter than that of the core-only nanoparticles, and the core-shell nanoparticles were used for bioimaging and drug delivery.[32] Zhen et al. successfully synthesized LaF_3: Er, Yb@ LaF_3 core-shell nanoparticles with un-doped shell and the luminescence lifetime of the core-shell nanoparticles were longer than that of the core nanoparticles, then core-shell nanoparticles were used to construct an Erbium-doped waveguide amplifier with a relative gain of ~3.5 dB at 1550 nm.[33] Furthermore, an active-core/active-shell approach was proposed to obtain NPs with strong emissions. In this case, an active shell (e.g., containing Yb^{3+} icons) was grown around the active core and could not only suppress surface quenching but also transfer the pump light to the core region efficiently via the active shell.[34-38] Yang et al. obtained $BaGdF_5$: Yb^{3+}, Tm^{3+}@ $BaGdF_5$: Yb^{3+} nanoparticles, and the luminescence intensity of NPs was obviously enhanced after coating with active-shell (containing Yb^{3+}). Then $BaGdF_5$: Yb^{3+}, Tm^{3+}@ $BaGdF_5$: Yb^{3+} nanoparticles were used for the invitro UC luminescence imaging of HeLa cells.[39] Zhai et al. reported a strategy to improve the intensity of the 1.53 μm fluorescent band in $BaYF_5$: Yb^{3+}, Er^{3+} NPs with the use of an active-shell (containing Yb^{3+}) and constructed an erbium doped waveguide amplifier based on $BaYF_5$: Yb^{3+}, Er^{3+} active-core–active-shell NPs with an enhanced optical gain of

~6.3 dB.[40] Recently, a multi-inert-layer coating method was employed to avoid the uneven shell coating for core-shell NPs,[41-43] Zhang et al. reported a reproducible method to grow a hexagonal $NaGdF_4$ shell on $NaYF_4$: Yb, Er nanocrystals with monolayer control thickness and direct imaging the up-conversion nanocrystal core/shell structure at the subnanometer level.[44] They also investigated the dependence of up-converting optical properties on shell thickness and doping position. The experimental results showed that the optical properties of the obtained core/shell NPs could be improved in up-conversion luminescence efficiency (up to 0.51%), stability (more resistant to quenching by water) and multicolour luminescence emission.[45] Very recently, Li et al. reported for the first time that the homogenous doping approach based on the successive layer-by-layer method can greatly improve the efficiency of UCNPs. The quantum yield as high as 0.89% was realized for the homogeneous doping $NaGdF_4$: Yb, Er@ $NaYF_4$ UCNPs.[46] Despite recent progress in this field, it is necessary to explore new approaches to achieve ultra-small NPs with improved efficiency for pushing forward the advance of this field.

In this paper, we reported an approach to improve the intensity of UC and DC fluorescence of $BaLuF_5$: Yb^{3+}, Er^{3+} NPs by using a multi-active-layer coating shell (containing Yb^{3+}). Sub-10 nm $BaLuF_5$: Yb^{3+}, Er^{3+}@ (X-shell, X=0~5) $BaLuF_5$: Yb^{3+} NPs were synthesized via a high boiling solvent process and a layer-by-layer strategy. In comparison with optical properties of the $BaLuF_5$: Yb^{3+}, Er^{3+} core-only NPs, the intensities of UC (~545 nm) and DC (~1530 nm) fluorescence were enhanced by 52 and 9.8 times after coating 5-layer active-shells ($BaLuF_5$: Yb^{3+}) on the $BaLuF_5$: Yb^{3+}, Er^{3+} NPs, respectively. To obtain more meaningful information about the active shells, a thick-layer active shell ($BaLuF_5$: Yb^{3+}) was coated on the $BaLuF_5$: Yb^{3+}, Er^{3+} core-only NPs and the resulting core-active thick shell NPs had a similar size as the NPs with 5-layer active shells. The intensities of UC and DC fluorescence of the $BaLuF_5$: Yb^{3+}, Er^{3+} NPs with multi-layer active-shells were 1.3 and 1.1 times larger than that of the $BaLuF_5$: Yb^{3+}, Er^{3+} NPs with one thick-layer active shell, respectively. The effects of the multi-layer active-shells on UC and DC fluorescence were also discussed.

Note that, here, $BaLuF_5$ compound was selected as the matrix due to its single crystalline phase. When the multi-layer shells were coated on the $BaLuF_5$ core NPs via a layer-by-layer strategy, the shells could grow epitaxially without any phase transition. Therefore, it was easy to analyze the effects of the multi-active-layer coating shells on the UC and DC properties of NPs.

2 Materials and Methods

2.1 Materials and general procedures

Ytterbium nitrate ($Yb(NO_3)_3$,99.99%), lutecium nitrate ($Lu(NO_3)_3$, 99.99%) and erbium nitrate ($Er(NO_3)_3$,99.99%) were bought from Beijing Chemicals Reagents, China. Oleic acid (OA) and 1-octadecene (ODE) were purchased from Alfa Aesar Company. Barium stearate was purchased from Stream Chemicals Inc. Sodium hydroxide (NaOH), stearic acid ($C_{17}H_{35}COOH$), and ammonium fluoride (NH_4F) with purity of A.R. were all obtained from Beijing Fine Chemical Company, China. The temporal properties were studied by using a 953.6 nm Raman shifter laser and an oscillograph. All chemicals were used without further purification.

2.2 Synthesis of $BaLuF_5$: Yb^{3+}, Er^{3+} core nanoparticles:

0.5mmol barium stearate and 0.5mmol pre-prepared rare-earth stearate (0.39mmol lutecium stearate,0.1mmol ytterbium stearate, 0.01mmol erbium stearate)[47] were added to a 100 mL four-necked flask containing 15 mL ODE and 15 mL OA. The solution was heated to 110 °C for 1 h under vacuum to remove any residual air.

Thereafter, the mixture was cooled to room temperature under argon (Ar) flow. 10 mL of methanol solution containing 3mmol NH_4F (about 111 mg) was added into the four-necked flask, then the system was kept at 50 °C for 30 min to remove methanol. Finally, the temperature was increased to 300 °C as soon as possible and the reactants was heated for 1 h under Ar flow, and then cooled to room temperature (RT). The NPs were washed and re-dispersed in cyclohexane. These NPs were used as cores to induce a subsequent shell coating.

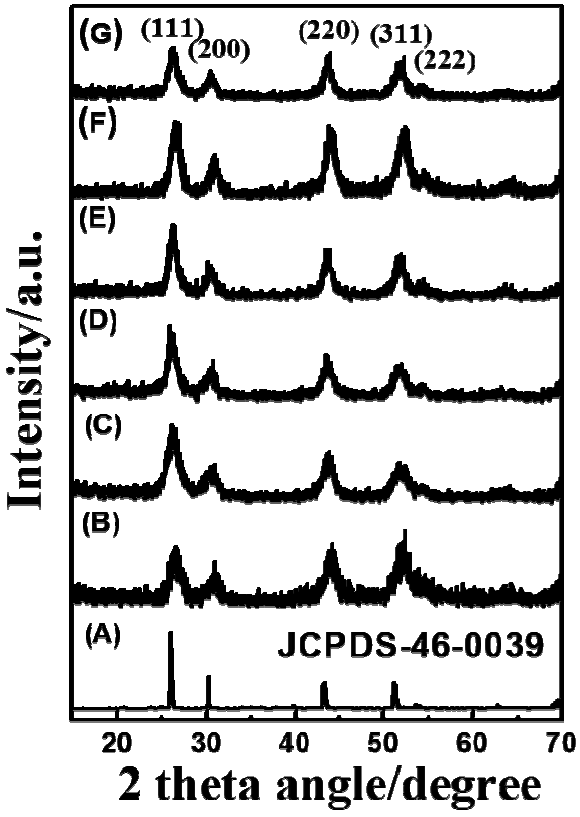

Fig. 1 XRD patterns of (A) standard $BaLnF_5$ NPs, (B) $BaLuF_5$: 20mol %Yb^{3+}, 2mol %Er^{3+} NPs, (C-G) $BaLuF_5$: 20mol %Yb^{3+}, 2mol %Er^{3+} @ (X-shell) $BaLuF_5$: 5mol %Yb^{3+} (x=1, 2, 3, 4, 5) NPs.

2.3 Synthesis of Multi-Shell $BaLuF_5$: Yb^{3+}, Er^{3+}@ $BaLuF_5$: Yb^{3+} Core–Shell Nanoparticle.

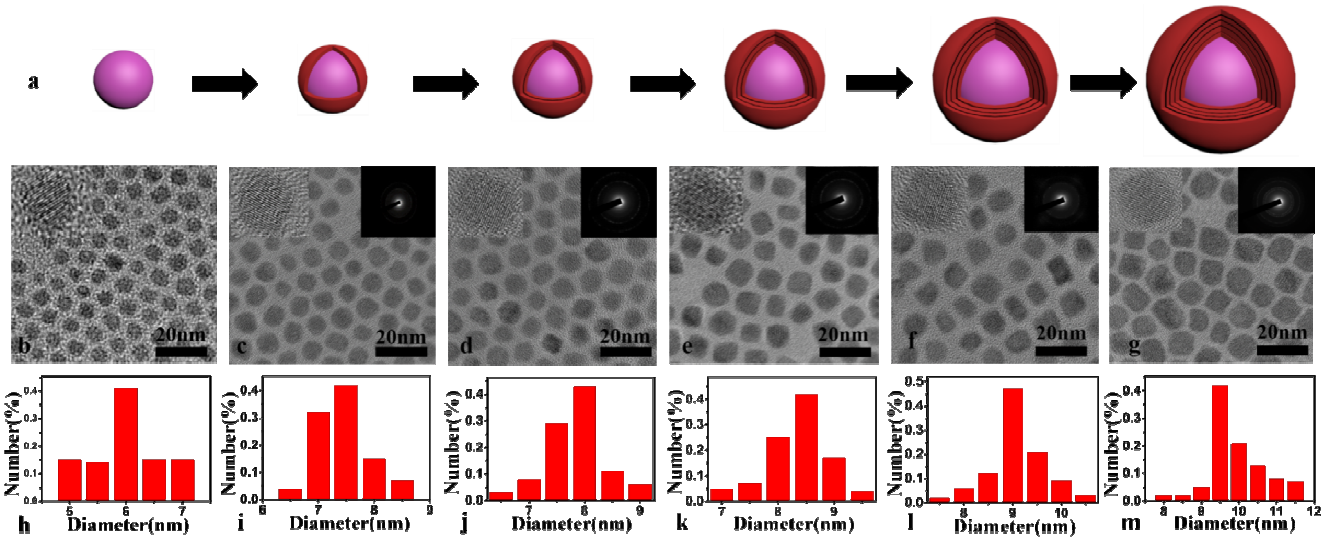

Fig. 2 (a) Schematic illustration of $BaLuF_5$: 20mol %Yb^{3+}, 2mol %Er^{3+} NPs and $BaLuF_5$: 20mol %Yb^{3+}, 2mol %Er^{3+}@ (X-shell) $BaLuF_5$: 5mol %Yb^{3+} (x=1, 2, 3, 4, 5) NPs. (b-g) TEM images of $BaLuF_5$: 20mol %Yb^{3+}, 2mol %Er^{3+}NPs and $BaLuF_5$: 20mol %Yb^{3+}, 2mol %Er^{3+} @ (X-shell) $BaLuF_5$: 5mol %Yb^{3+} (x=1, 2, 3, 4, 5) NPs. (Insets: corresponding high-resolution TEM image and SAED). (h-m) Size distribution of $BaLuF_5$: 20mol %Yb^{3+}, 2mol %Er^{3+} and $BaLuF_5$: 20mol %Yb^{3+}, 2mol %Er^{3+} @ (X-shell) $BaLuF_5$: 5mol %Yb^{3+} (x=1, 2, 3, 4, 5) NPs.

The core−shell $BaLuF_5$: Yb^{3+}, Er^{3+}@ $BaLuF_5$: Yb^{3+} nanoparticles were synthesized through a modified high boiling solvent process. 0.5mmol shell precursors (0.475mmol lutecium stearate, 0.025mmol ytterbium stearate) were added to a 100 mL four-necked flask containing 15 mL ODE and 15 mL OA. This mixture was heated to 110 °C for 30 min under Ar flow to form a clear solution and then cooled down to 60 °C. Subsequently, the core NPs cyclohexane solution was added into the system flask under stirring system and the mixture was heated to 80 °C for 30 min to remove cyclohexane. 10 mL of methanol solution containing 3mmol NH_4F (about 111 mg) was added into the flask and then the system was kept at 50°C for 30 min to remove methanol. Finally, the mixture was heated to 300 °C for 1 h under Ar flow with vigorous stirring. The flask was then cooled to RT. These core-shell NPs with one layer were precipitated, washed, and re-dispersed in cyclohexane. To coat the second layer of the active shell, these as-synthesized core-shell NPs were used as seeds. The same coating process was repeated for other four times until the original $BaLuF_5$: Yb^{3+}, Er^{3+} NPs were coated with five layers.

For comparison, we also synthesized $BaLuF_5$: Yb^{3+}, Er^{3+} NPs with one thick-layer active shell. The reaction time of shell coating was prolonged for 1.5 h to obtain thick shell.

2.4 Characterization

The phase of the samples was characterized by X-ray powder diffraction (XRD) (Model Rigaku Ru-200b), using a nickel-filtered Cu-K α radiation (λ = 1.5406 Å) the 2θ angle ranges of 10 °⩽2θ⩽70 °.The transmission electron microscopy (TEM) images, high-resolution TEM (HRTEM) images and the energy dispersive X-ray spectrometry (EDX) of the samples were obtained by a JEM-2100F electron microscope at 200 kV. Up-conversion spectra were recorded using a Hitachi F-4500 fluorescence spectrophotometer (1.0 nm for slit resolution and 700 V for PMT voltage), and DC spectra were gotten using a SPEX 1000M spectrometer (2 mm for slit width). All spectra were obtained using a 980 nm continuous laser diode as the excitation source. The temporal properties were studied by using a 953.6 nm Raman shifter laser and an oscillograph. All the measurements were performed at room temperature.

We successfully synthesized $BaLuF_5$: Yb^{3+}, Er^{3+}core nanoparticles via a high boiling solvent process, and prepared $BaLuF_5$: Yb^{3+}, Er^{3+}@ (X-shell, X=1~5) $BaLuF_5$: Yb^{3+} NPs through an epitaxial growth process. Fig. 1 shows X-ray

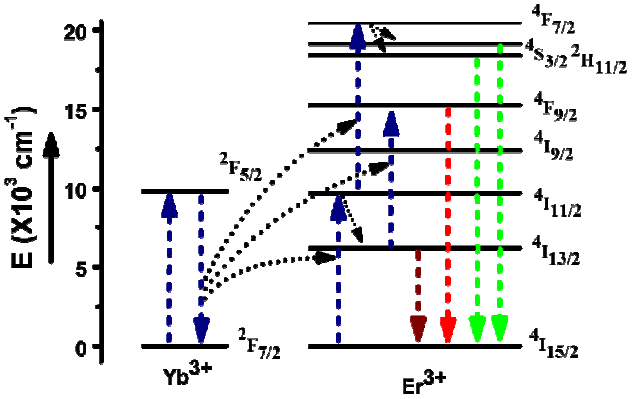

Fig. 3 Energy-level diagram of Yb^{3+} and Er^{3+}, possible up-conversion and down-conversion processes under excitation of a 980 nm laser diode.

diffraction (XRD) patterns of $BaLuF_5$: 20mol%Yb^{3+}, 2mol%Er^{3+} and $BaLuF_5$: 20mol%Yb^{3+}, 2mol%Er^{3+}@ (X-shell) $BaLuF_5$: 5mol%Yb^{3+} (x=1, 2, 3, 4, 5) NPs with different numbers of shells, respectively. The diffraction peaks coincide well with the literature values (JCPDS NO. 46-0039). The diffraction peaks at 26.4°, 30.5°, 43.8°and 51.5°can be ascribed to the (131), (330), (123), and (062) planes. The diffraction peaks of the samples can be indexed to tetragonal phase $BaLuF_5$, and the NPs are $BaLuF_5$ nanoparticles. To further confirm the composition of the samples,

the energy dispersive X-ray spectrometry (EDX) of the $BaLuF_5$: 20mol%Yb^{3+}, 2mol%Er^{3+}@ $BaLuF_5$: 5mol%Yb^{3+} NPs was measured and shown in Fig. S1. The existence of Ba, Lu, Yb, F and Er elements were clarified by EDX spectrum of the NPs (Fig. S1). To characterize the morphology of the samples, TEM images, and High-resolution TEM images were measured. Fig. 2a show schematic illustration of $BaLuF_5$: Yb^{3+}, Er^{3+} core nanoparticles and $BaLuF_5$: Yb^{3+}, Er^{3+}@ (X-shell, X=1~5) $BaLuF_5$: Yb^{3+} NPs. Fig. 2b–2g are the TEM images of the $BaLuF_5$: Yb^{3+}, Er^{3+} core nanoparticles and $BaLuF_5$: Yb^{3+}, Er^{3+}@ (X-shell, X=1~5) $BaLuF_5$: Yb^{3+} NPs and Selected area electron diffraction (SAED)

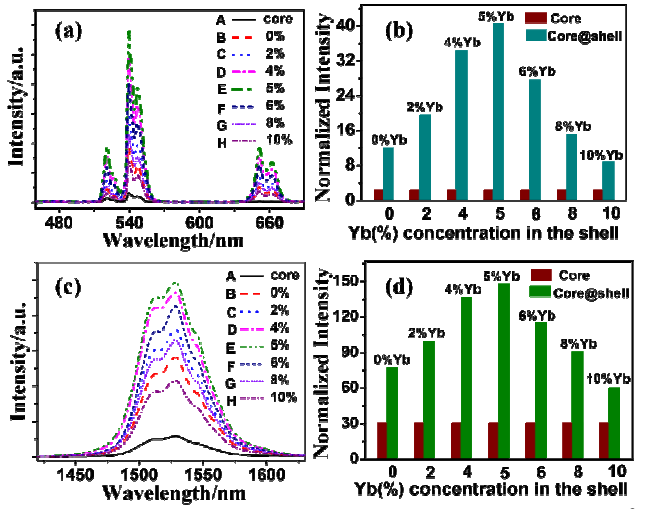

Fig.4 Dependence of the UC and DC emission intensities on the Yb^{3+} concentration in the shells. (a) UC and (c) DC emission spectra of $BaLuF_5$: 20mol%Yb^{3+}, 2mol %Er^{3+} NPs (curve A) and $BaLuF_5$: 20mol%Yb^{3+}, 2mol%Er^{3+}@ $BaLuF_5$: xmol%Yb^{3+} (x= 0, 2, 4, 5, 6, 8, 10) NPs (curve B-H) under a 980 nm excitation. Intensity enhancement of (b) UC and (d) DC emission depending on the Yb^{3+} concentrations in the shell.

in each image. No obvious aggregation was observed, because there are hydrophobic OA ligands capping on the NPs. And the nanoparticles have uniform morphology, which are likely attributed to the interaction of their surface surfactants. Histograms of the size distribution of $BaLuF_5$: Yb^{3+}, Er^{3+} core nanoparticles and $BaLuF_5$: Yb^{3+}, Er^{3+}@ (X-shell, X=1~5) $BaLuF_5$: Yb^{3+} NPs are shown in Fig. 2h–2m. As we can see from Fig. 2b and Fig. 2h $BaLuF_5$: Yb^{3+}, Er^{3+} core nanoparticles are uniform roughly spherical and the average size is about ~6nm. Fig. 2c-2g and Fig. 2i-2m show TEM images and the size distribution of NPs fabricated through a layer-by-layer strategy, The size of $BaLuF_5$: Yb^{3+}, Er^{3+}@ (X-shell, X=1~5) $BaLuF_5$: Yb^{3+} NPs gradually increases from 6 to 10 nm with increasing the number of layers.

3. Results and discussions

3.1 Dependence of the UC and DC properties of $BaLuF_5$: 20mol%Yb^{3+}, 2mol %Er^{3+}@ $BaLuF_5$: Yb^{3+} NPs on the Yb^{3+} concentration of the shell

It is known that Yb^{3+} is commonly chosen as a sensitizer for UC materials owing to its large absorption cross-section at 980 nm. In Yb^{3+}-Er^{3+} co-doped systems (shown in Fig. 3), with the excitation of a 980 nm laser diode, energy transfer from Yb^{3+} to Er^{3+} occurs because of the large spectral overlap between the $^2F_{5/2}\rightarrow{}^2F_{7/2}$ transition of Yb^{3+} and the $^4I_{15/2}\rightarrow{}^4I_{11/2}$ absorption of Er^{3+}, which results in the population of the $^4I_{11/2}$ level. Then electrons on the $^4I_{11/2}$ level relax non-radiatively to the $^4I_{13/2}$ level and the $^4I_{13/2}\rightarrow{}^4I_{15/2}$ transition gives the DC emission at 1.53 μm. Furthermore, Yb^{3+} ions continuously absorb 980 nm photons and transfer the energy to Er^{3+} to populate high energy levels of Er^{3+} ions and the transitions from high energy levels to the ground state of Er^{3+} give various UC emissions. It is clearly that DC and UC properties of Yb^{3+}-Er^{3+} co-doped materials can be affected by the doping concentration of Yb^{3+} and Er^{3+} ions. In our experiments, we firstly optimized the doping concentration of Yb^{3+} or Er^{3+} ions in $BaLuF_5$ core NPs for obtaining strong DC and UC emissions. The optimized values were 20% and 2%, respectively.[40]

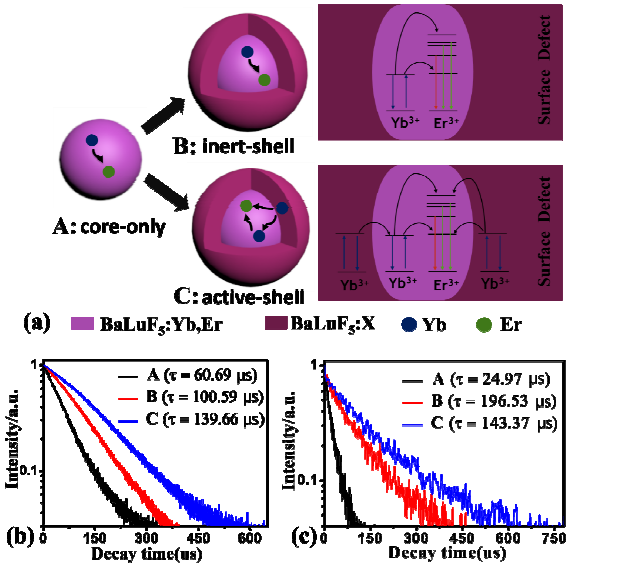

Fig. 5 Influence of Yb^{3+} doping in the shell on the UC and DC emissions. (a) Schematic illustration and energy transfer mechanisms of NPs with inert-shell (no Yb^{3+}) and active-shell (Yb^{3+} doping). (b) Photoluminescence decay curves of the $^4S_{3/2}$ level of Er^{3+} in (A) core NPs, (B) core-inert-shell NPs and (C) core-active-shell NPs. (c) Photoluminescence decay curves of the $^2F_{5/2}$ level of Yb^{3+} in (A) core NPs, (B) core-inert-shell NPs and (C) core-active-shell NPs.

By using $BaLuF_5$: 20mol %Yb^{3+}, 2mol %Er^{3+} NPs as the core, we prepared $BaLuF_5$: 20mol %Yb^{3+}, 2mol %Er^{3+}@ $BaLuF_5$: Yb^{3+} active-core-active-shell NPs with varied Yb^{3+} concentration in the shell. To make sure of the interaction between Yb^{3+} in the shell and active ions in the core region, the thickness of the shell was fixed at 0.7 nm for those samples. To clarify the effects of the Yb^{3+} concentration in the shell on optical properties of NPs, we measured UC, DC emission spectra and enhancement ratio of UC, DC luminescence of $BaLuF_5$: 20mol%Yb^{3+}, 2mol%Er^{3+}@ $BaLuF_5$: Yb^{3+} NPs with varied Yb^{3+} concentration in the shell under the excitation of a 980 nm laser diode with a fixed power density of 70 W cm^{-2}, as shown in Fig. 4. Three emissions peaked at 525, 545 and 650 nm were observed in the UC emission spectra (shown in Fig. 4a), which were attributed to the $^2H_{11/2}\rightarrow{}^4I_{15/2}$, $^4S_{3/2}\rightarrow{}^4I_{15/2}$ and $^4F_{9/2}\rightarrow{}^4I_{15/2}$ transitions of Er^{3+}, respectively. One emission peaked at 1530 nm which originated from the $^4I_{13/2}\rightarrow{}^4I_{15/2}$ transition of Er^{3+} was observed in the DC emission spectra (shown in Fig. 4c). After coating an inert shell $BaLuF_5$ on the core NPs, the UC and DC emissions were enhanced by 4.9 and 2.5 times compared to that of the core-only NPs owing to the well-known surface passivation effect of the

shell, respectively. In the case of $BaLuF_5$: 20mol%Yb^{3+}, 2mol%Er^{3+}@ $BaLuF_5$: Yb^{3+} active-core-active-shell NPs, the intensity of the UC or DC emissions increased monotonically to the corresponding maximum value with increasing the Yb^{3+} concentration of the shell from zero to 5mol%. Furthermore, the intensity of the UC or DC emissions decreased gradually with increasing the Yb^{3+} concentration of the shell from 5% to 10%. Thus, the optimum concentration of Yb^{3+} in the shell was about 5mol% for the active-core-active-shell NPs. The above results showed that by doping a certain amount (e.g., ~5mol%) of Yb^{3+} ions into the shell, the UC and DC emissions of $BaLuF_5$: 20mol%Yb^{3+}, 2mol%Er^{3+}@ $BaLuF_5$: 5mol%Yb^{3+} active-core-active-shell NPs were further improved by 3.3 and 1.9 times compared to that of $BaLuF_5$: 20mol %Yb^{3+}, 2mol %Er^{3+}@ $BaLuF_5$ active-core-inert-shell NPs since the Yb^{3+} ions in the shell could transfer energy from the pump source to the core and make a contribution to the UC and DC emissions. However, if the Yb^{3+} concentration in the shell was too high (>5mol%), the Yb^{3+} ions in the shell would preclude the core region from the excitation of the 980 nm laser diode and also the concentration quenching effect occurred, causing the weakening of the UC and DC emissions.

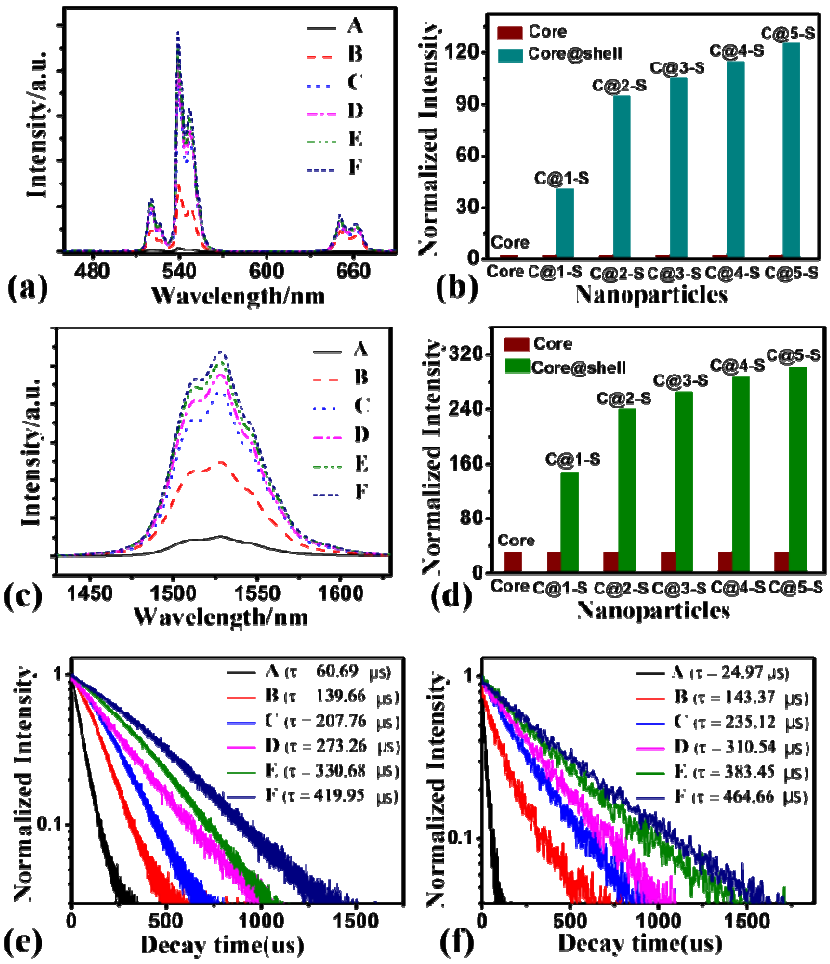

Fig. 6 Influence of the number of the active shell layers on the UC and DC properties. (a) UC and (c) DC luminescence spectra of core NPs (A) and core-shell NPs with X-layer shell (x=0, 1, 2, 3, 4, 5) (B-F) under a 980 nm laser excitation. Intensity enhancement of (b) UC and (d) DC emission depending on the number of the active-shell layers. (e) Photoluminescence decay curves of the $^4S_{3/2}$ level of Er^{3+} in (A) core NPs and (B-F) core-shell NPs with X-layer shell (x=1, 2, 3, 4, 5). (f) Photoluminescence decay curves of $^2F_{5/2}$ level of Yb^{3+} in (A) core NPs and (B-F) core-shell NPs with X-layer shell (x=1, 2, 3, 4, 5).

In addition, we measured the lifetime of the $^2F_{5/2}$ level of Yb^{3+} and the $^4S_{3/2}$ level of Er^{3+} in $BaLuF_5$: 20mol%Yb^{3+}, 2mol%Er^{3+}(core-only), $BaLuF_5$: 20mol%Yb^{3+}, 2mol %Er^{3+}@ $BaLuF_5$ (active-core-inert-shell) or $BaLuF_5$: 20mol%Yb^{3+}, 2mol%Er^{3+}@ $BaLuF_5$: 5mol%Yb^{3+} (active-core-active-shell) NPs by using a 953.6 nm pulsed laser with a pulse width of 10 ns and a repetition rate of 10 Hz as the excitation source, respectively. The measured data were shown in Fig. 5b and 5c. Each of the decay curves can be fitted well with a single-exponential function as $I = I_0 \exp(-t/\tau)$, where I_0 is the initial emission intensity at t = 0 and τ is the lifetime of the monitored level. By growing an inert shell on the core NP, the lifetime of the $^4S_{3/2}$ or $^2F_{5/2}$ level was extended from 60.69 μs to 100.59 μs or 24.97 μs to 96.53 μs owing to the reduction of the nonradiative relaxation rate caused by the surface passivation effect. Interestingly, the lifetime of the $^4S_{3/2}$ and $^2F_{5/2}$ level was further increased to 139.66 μs and 143.37 μs by introducing Yb^{3+} ions into the shell to form the active shell. In this case, there are two factors that contribute to the increase of the lifetime. One is the surface passivation effect. The other is originated from Yb^{3+} ions inside the shell. Since the Yb^{3+} concentration of the shell was lower than that of the core region, the lifetime of the $^2F_{5/2}$ level of Yb^{3+} in the shell would be longer

than that in the core region.[48,49] Therefore, the lifetime of the $^2F_{5/2}$ level for the $BaLuF_5$: 20mol%Yb^{3+}, 2mol%Er^{3+}@ $BaLuF_5$: Yb^{3+} NPs was longer than that for the $BaLuF_5$: 20mol%Yb^{3+}, 2mol %Er^{3+}@ $BaLuF_5$ NPs. Generally, the measured lifetime of the $^4S_{3/2}$ level of Er^{3+} in Yb^{3+} and Er^{3+} codoped systems pumped at 953.6 nm is related to the lifetime of the $^2F_{5/2}$ level of Yb^{3+} owing to the existence of energy transfer from Yb^{3+} to Er^{3+}. As aforementioned, the lifetime of the $^4S_{3/2}$ level of Er^{3+} was further increased to 139.66 μs by introducing Yb^{3+} ions into the shell to form the active shell. So we concluded that the increase of the lifetime of the $^4S_{3/2}$ level of Er^{3+} was caused by the contribution of energy transfer from Yb^{3+} ions inside the shell to Er^{3+} ions in the core region. In other words, it was an evidence that energy transfer from Yb^{3+} ions inside the shell to the core region occurred. Generally, for Yb^{3+} and Er^{3+} co-doped systems, the longer the lifetime of the $^2F_{5/2}$ or $^4S_{3/2}$ level is, the stronger the UC or DC emission becomes. Therefore, the increase of the lifetime of $^4S_{3/2}$ or $^2F_{5/2}$ level might cause the enhancement of the UC or DC emission by growing an active shell on the core NP, which was consistent with the measured UC or DC emission spectra shown in Fig. 5b and 5c.

3.2 Influence of the number of the active shell layers on the UC and DC properties of $BaLuF_5$: 20mol%Yb^{3+}, 2mol %Er^{3+}@ (X-shell) $BaLuF_5$: 5mol %Yb^{3+} (X= 1, 2, 3, 4, 5) NPs

To investigate the influence of the number of shell layers on optical properties of NPs, we synthesized $BaLuF_5$: 20mol%Yb^{3+}, 2mol%Er^{3+}@ (X-shell) $BaLuF_5$: 5mol %Yb^{3+} (X= 0, 1, 2, 3, 4, 5) NPs via the layer-by-layer strategy (shown in Fig. 2) and characterized their UC and DC properties. By increasing the number of the active shell layers from 0 to 5, the average size of NPs increased gradually from 6 to 9.5 nm and the uniformity of NPs kept almost unchanged with an increase of the size. The above results indicated that multi-layer active-shell grew uniformly on the core NPs via the layer-by-layer strategy. Figure 6a, 6c and 6b, 6d shows the measured UC, DC emission spectra and enhancement ratio of UC, DC luminescence of $BaLuF_5$: 20mol%Yb^{3+}, 2mol%Er^{3+}@ (X-shell) $BaLuF_5$: 5mol%Yb^{3+} (X= 0, 1, 2, 3, 4, 5) under the excitation of a 980 nm laser diode with a fixed power density of 70 W cm^{-2}. By increasing the number of the shell layers from 0 to 2, the UC and DC emission increased monotonically and the corresponding rate of increase was 38.25 and 6.81 times per layer, respectively. Interestingly, with further increasing the number of the shell layers from 2 to 5, the rate of increase for the UC or DC emission reduced to 0.32 or 0.26 times per layer, respectively. The above results showed that multi-layer active-shells could be used to not only suppress surface quenching but also transfer energy from the pump light to the core region efficiently through Yb^{3+} ions inside the active-shells, causing the enhancement of the UC or DC emission. Especially, since the thickness of each shell layer was about 0.7 nm, one shell layer was not enough for suppressing completely surface quenching. In addition, Yb^{3+} ions in each shell layer could absorb the pump light and transfer energy to the core region. As a result, the initial increase (0→2) of the number of the shell layers caused the obvious improvement of the UC or DC emission. However, by further increasing the number of the shell layers (2→5), the suppression effect of surface quenching became weak and the energy transfer from Yb^{3+} ions in the outer shell layers to the core region became inefficient owing to the enlargement of the distance between them, which made the rate of increase for the UC or DC emission smaller.

Figure 6e and 6f show the measured lifetime of the $^2F_{5/2}$ level of Yb^{3+} and the $^4S_{3/2}$ level of Er^{3+} in $BaLuF_5$: 20mol%Yb^{3+}, 2mol%Er^{3+}@ (X-shell) $BaLuF_5$: 5mol%Yb^{3+} (X= 0, 1, 2, 3, 4, 5) NPs by using a 953.6 nm pulsed laser with a pulse width of 10 ns and a repetition rate of 10 Hz as the excitation source. With increasing the number of the shell layers from 0 to 5, the lifetime of the $^4S_{3/2}$ and $^2F_{5/2}$ level was increased from 60.69 μs to 419.95 μs and 24.97 μs to 464.66 μs owing to the suppression of surface quenching and the contribution of Yb^{3+} ions inside the shell to the lifetime of the $^4S_{3/2}$ or $^2F_{5/2}$ level, which agreed well with the tendency toward the dependence of the measured UC and DC emissions on the number of the shell layers (shown in Fig. 6b and 6d).

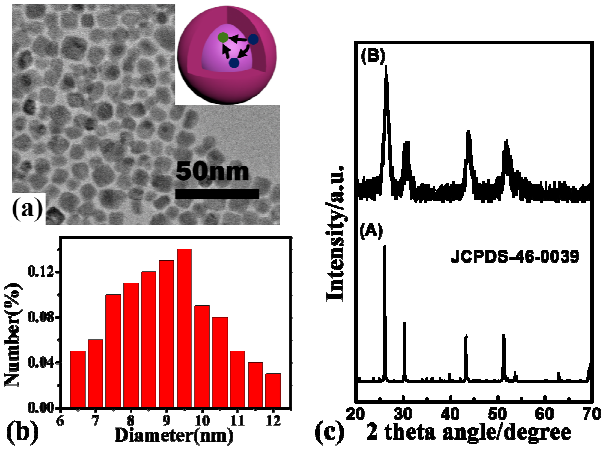

Fig. 7 $BaLuF_5$: 20mol%Yb^{3+}, 2mol%Er^{3+}@ $BaLuF_5$: 5mol%Yb^{3+} NPs with one thick active shell as the control. (a) TEM images of the control NPs. (b) Size distribution of the control NPs. (c) XRD patterns of (A) standard $BaLnF_5$ crystals and (B) the control NPs.

Note that, we also synthesized $BaLuF_5$: 20mol%Yb^{3+}, 2mol%Er^{3+}@ (X-shell) $BaLuF_5$: 5mol%Yb^{3+} (X≥6) NPs via the layer-by-layer strategy. Since the size of those NPs was larger than 10 nm, they were out of scope that we were interested in.

3.3 Comparisons of the UC and DC properties of $BaLuF_5$: 20mol %Yb^{3+}, 2mol %Er^{3+}@ (5-shell) $BaLuF_5$: 5mol%Yb^{3+} NPs and $BaLuF_5$: 20mol%Yb^{3+}, 2mol%Er^{3+}@ $BaLuF_5$: 5mol%Yb^{3+} NPs with the similar shell thickness.

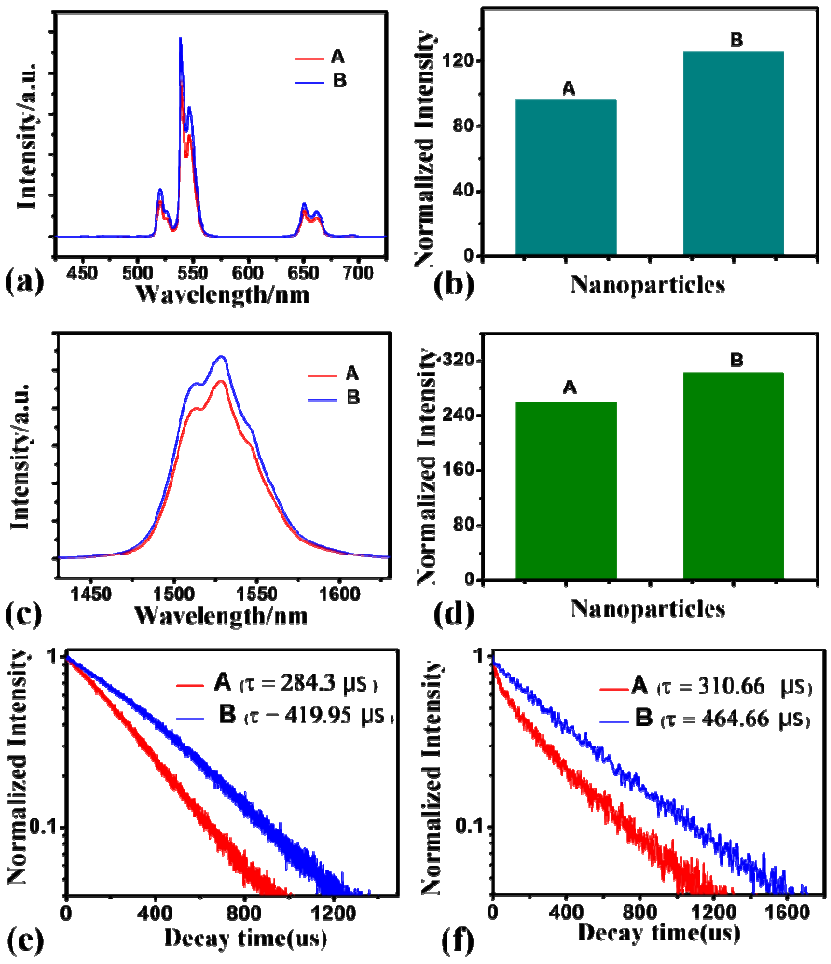

Fig. 8 Comparisons of the UC and DC properties of $BaLuF_5$: 20mol %Yb^{3+}, 2mol %Er^{3+}@ (5-shell) $BaLuF_5$: 5mol%Yb^{3+} NPs and $BaLuF_5$: 20mol%Yb^{3+}, 2mol%Er^{3+}@ $BaLuF_5$: 5mol%Yb^{3+} NPs with the similar shell thickness. (a) UC and (c) DC emission spectra of NPs with 5-layer shells and the control NPs with one thick shell under a 980 nm laser excitation. Intensity enhancement of (b) UC and (d) DC emission. (e) Photoluminescence decay curves of $^4S_{3/2} \rightarrow {}^4H_{15/2}$ transitions of Er^{3+} in NPs with 5-layer shells (A) and the control NPs with one thick shell (B). (f) Photoluminescence decay curves of $^2F_{5/2} \rightarrow {}^2H_{7/2}$ transitions of Yb^{3+} in NPs with 5-layer shells (A) and the control NPs with one thick shell (B).

Although $BaLuF_5$: 20mol%Yb^{3+}, 2mol%Er^{3+}@ (5-shell) $BaLuF_5$: 5mol%Yb^{3+} NPs gives rise to improved UC and DC emissions compared to the $BaLuF_5$: 20mol%Yb^{3+}, 2mol%Er^{3+} core-only NPs, is it exactly better than $BaLuF_5$:20mol %Yb^{3+}, 2mol%Er^{3+} @ $BaLuF_5$: 5mol%Yb^{3+} NPs with the similar size and shell thickness of 3.5nm. To clarify this question, we prepared $BaLuF_5$: 20mol%Yb^{3+}, 2mol %Er^{3+}@ $BaLuF_5$: 5mol %Yb^{3+} NPs with the similar size and shell thickness (shown in Fig. 7a) as that of $BaLuF_5$: 20mol%Yb^{3+}, 2mol%Er^{3+}@ (5-shell) $BaLuF_5$: 5mol %Yb^{3+} NPs. Fig. 7a and 7b show TEM image and the size-distribution of the as-prepared sample. The average size was about 9.5 nm, which is similar as that of $BaLuF_5$: 20mol%Yb^{3+}, 2mol%Er^{3+}@ (5-shell) $BaLuF_5$: 5mol%Yb^{3+} NPs. However, the uniformity of the as-prepared sample was worse than that of $BaLuF_5$: 20mol%Yb^{3+}, 2mol%Er^{3+}@ (5-shell) $BaLuF_5$: 5mol%Yb^{3+} NPs. This result also showed that we could obtain uniform active-core-active-shell NPs by using a layer-by-layer strategy. Fig. 7c shows XRD pattern of the as-prepared sample. The diffraction peaks of the as-prepared sample can be indexed as tetragonal phase $BaLuF_5$. Fig. 8a, 8c and 8b, 8d show a comparison of the UC, DC emission spectra and enhancement ratio of UC, DC luminescence of $BaLuF_5$: 20mol%Yb^{3+}, 2mol%Er^{3+}@ (5-shell) $BaLuF_5$: 5mol%Yb^{3+} NPs and $BaLuF_5$: 20mol%Yb^{3+}, 2mol%Er^{3+}@ $BaLuF_5$: 5mol%Yb^{3+} NPs with the similar shell thickness measured by using a 980 nm laser diode with a fixed power density of 70 W cm^{-2} as the pump source. The UC and DC emissions of the former NPs with multi-layer active-shells were 1.3 and 1.1 times larger than that of the latter NPs with one thick-layer active shell, respectively. Figure 8e and 8f show a comparison of the measured lifetime of the $^4S_{3/2}$ and $^2F_{5/2}$ level of those two samples. The lifetime of the $^4S_{3/2}$ and $^2F_{5/2}$ level of the NPs with multi-layer active-shells were 1.47 and 1.49 times longer than that of the NPs with one thick-layer active shell. We considered that, for the NPs with one thick-layer active shell prepared by one-step coating method, surface defects of NPs cannot be completely passivated by the one-step shell deposition process. In contrast, during the growth of the $BaLuF_5$: 5mol%Yb^{3+} shell layer by layer, surface defects of NPs can be gradually passivated by the homogeneous shell deposition process, which results in the obvious enhancement in overall UC or DC emission intensity and lifetime compared to that of the NPs with one thick-layer active shell.[45,46] The above results

showed that we could obtain sub-10 nm NPs with good size-uniformity and improved UC or DC fluorescence by using a multi-active-layer coating shell containing Yb^{3+} ions.

4. Conclusion

In summary, we proposed an approach to improve the intensity of UC and DC fluorescence of ultra-small $BaLuF_5$: Yb^{3+}, Er^{3+} NPs by using a multi-active-layer coating shell containing Yb^{3+} ions. Sub-10 nm $BaLuF_5$: Yb^{3+}, Er^{3+}@ (5-shell) $BaLuF_5$: Yb^{3+} NPs were synthesized via a layer-by-layer strategy. In comparison with optical properties of the $BaLuF_5$: Yb^{3+}, Er^{3+} core-only NPs, the intensities of UC (~545 nm) and DC (~1530 nm) fluorescence were enhanced by 52 and 9.8 times after coating 5-layer active-shells ($BaLuF_5$: Yb^{3+}) on the $BaLuF_5$: Yb^{3+}, Er^{3+} NPs, respectively. Our experimental results showed that multi-layer active-shells could be used to not only suppress surface quenching but also transfer the pump light to the core region efficiently through Yb^{3+} ions inside the active-shells. Sub-10 nm active-core-multi-active-layer-shell NPs with good uniformity and improved UC or DC fluorescence could be obtained by the homogeneous shell deposition process.

Acknowledgments

This work was supported by NSFC (grants 61178073, 11274139, 61222508, 61275189, 61378004, 60908001, 61077033, 51072065 and 60908031), the Opened Fund of the SKLIO, and TNList Cross-discipline Foundation, SRG2013-00035-FHS Grant and MYRG2014-00093-FHS Grant from University of Macau in Macau.

Notes and references

[a] *Opto-electronic, College of Electronic Science & Engineering, Jilin University, Changchun 130012, China. Fax: +86 4318516 8241; Tel: +86 431 8516 8325; E-mail: dzhao@jlu.edu.cn; qings@jlu.edu.cn; wpqin@jlu.edu.cn .*

[b] *Bioimaging Core, Faculty of Health Science, University of Macau, Taipa, Macau SAR China.*

† Electronic Supplementary Information (ESI) available: [details of any supplementary information available should be included here]. See DOI: 10.1039/b000000x/

‡ Footnotes should appear here. These might include comments relevant to but not central to the matter under discussion, limited experimental and spectral data, and crystallographic data.

1. Guo-Bin Shan, George P. Demopoulos, Adv. Mater., 2010, 22, 4373
2. Ziyao Zhou, Jiahong Wang, Fan Nan, Chenghao Bu, Zhenhua Yu, Wei Liu, Shishang Guo, Hao Hu, Xing-Zhong Zhao, Nanoscale, 2014,6, 2052
3. Ka-Long Lei, Cheuk-Fai Chow, Kwok-Chu Tsang, Elva N. Y. Lei, V. A. L. Roy, Michael H. W. Lam, C. S. Lee,a E. Y. B. Punc, Jensen Li, J. Mater. Chem., 2010, 20, 7526
4. S. Bo, J.Wang, H. Zhao, H. Ren, Q.Wang, G. Xu, X. Zhang, X. Liu, Z. Zhen, Appl. Phys. B, 2008, 91, 79
5. N. M. Idris, M. K. Gnanasammandhan, J. Zhang, P. C. Ho, R. Mahendran, Y. Zhang, Nat. Med., 2012, 18, 1580
6. Weiping Qin, Daisheng Zhang, Dan Zhao, Lili Wang, Kezhi Zheng, Chem. Commun., 2010, 46, 2304
7. Feng Wang, Yu Han, Chin Seong Lim, Yunhao Lu, Juan Wang, Jun Xu, Hongyu Chen, Chun Zhang, Minghui Hong, Xiaogang Liu, Nature, 2010, 463, 1061
8. Yan-Mei Wu, Yao Cen, Li-Jiao Huang, Ru-Qin Yu and Xia Chu, Chem. Commun., 2014,50, 4759
9. Yun Sun, Xingjun Zhu, Juanjuan Peng, Fuyou Li, ACS Nano, 2013, 7 (12), 11290
10. Qingqing Dou, Niagar, Muhammad Idris, Yong Zhang, Biomaterials, 2013, 34(6), 1722
11. Gan Tian, Wenyan Yin, Junjiang Jin, Xiao Zhang, Gengmei Xing, Shoujian Li, Zhanjun Gu, Yuliang Zhao, J. Mater. Chem. B, 2014, 2, 1379
12. Wenyan Yina, Gan Tiana, Wenlu Ren, Liang Yan, Shan Jina, Zhanjun Gua, Liangjun Zhou,, Juan Li, Yuliang Zhao, Dalton Trans., 2014, 43, 3861
13. Juanjuan Peng, Yun Sun, Lingzhi Zhao, Yongquan Wu, Wei Feng,Yanhong Gao, Fuyou Li, Biomaterials, 2013, 34, 9535
14. Li Zhou, Zhenhua Li, Zhen Liu, Meili Yin, Jinsong Ren, Xiaogang Qu, Nanoscale, 2014, 6, 1445
15. Liang Cheng, Kai Yang, Shuai Zhang, Mingwang Shao, Shuittong Lee, Zhuang Liu, Nano Res., 2010, 3(10), 722
16. Liang Cheng, Kai Yang, Yonggang Li, Jianhua Chen, Chao Wang, Mingwang Shao, Shuit-Tong Lee, Zhuang Liu, Angewandte Chemie, 2011, 123(32), 7523
17. Heike S Mader, Peter Kele, Sayed M Saleh, Otto S Wolfbeis, Current opinion in chemical biology, 2010, 14(5), 582
18. Xiaomin Li, Rui Wang, Fan Zhang, Lei Zhou, Dengke Shen, Chi Yao , Dongyuan Zhao, Scientific reports, 2013, 3.
19. Lei Lei, Daqin Chen, Feng Huang, Yunlong Yu, Yuansheng Wang, Journal of Alloys and Compounds, 2012, 540, 27.
20. Wei Zheng, Shanyong Zhou, Zhuo Chen, Ping Hu, Yongsheng Liu, Datao Tu, Haomiao Zhu, Renfu Li, Mingdong Huang, Xueyuan Chen, Angew. Chem. 2013, 125, 6803
21. Songjun Zeng, Ming-Kiu Tsang, Chi-Fai Chan, Ka-Leung Wong, Bin Feid, Jianhua Hao, Nanoscale, 2012, 4, 5118
22. Guanying Chen, Tymish Y. Ohulchanskyy, Wing Cheung Law, Hans Agren, Paras N. Prasad, Nanoscale, 2011, 3, 2003
23. Hon-Tung Wong, Fiorenzo Vetrone, Rafik Naccache, Helen Lai Wa Chan, Jianhua Hao, John A. Capobianco, J. Mater. Chem., 2011, 21, 16589
24. Guanying Chen, Jie Shen, Tymish Y. Ohulchanskyy, Nayan J. Patel, Artem Kutikov, Zhipeng Li, Jie Song, Ravindra K. Pandey, Hans Agren, Paras N. Prasad, Gang Han, ACS nano, 2012, 6(9), 8280
25. Yu Wang, Langping Tu, Junwei Zhao, Yajuan Sun, Xianggui Kong, Hong Zhang, J. Phys. Chem. C, 2009, 113, 7164
26. Guanying Chen, Tymish Y. Ohulchanskyy, Sha Liu, Wing-Cheung Law, Fang Wu, Mark T. Swihart, Hans Agren, Paras N. Prasad, ACS nano, 2012, 6(4), 2969
27. Keith A. Abel, John-Christopher Boyer, Carmen M. Andrei, Frank C. J. M. van Veggel, J. Phys. Chem. Lett., 2011, 2, 185
28. Shan Jin, Liangjun Zhou, Zhanjun Gu, Gan Tian, Liang Yan, Wenlu Ren, Wenyan Yin, Xiaodong Liu, Xiao Zhang, Zhongbo Huc, Yuliang Zhao, Nanoscale, 2013, 5(23), 11910
29. Marina M. Lezhnina, Thomas Jüstel, Heike Kätker, Detlef U. Wiechert, Ulrich H. Kynast, Adv. Funct. Mater., 2006, 16, 935
30. Shili Gai, Piaoping Yang, Xingbo Li, Chunxia Li, Dong Wang, Yunlu Daib, Jun Lin, J. Mater. Chem., 2011, 21, 14610
31. John-Christopher Boyer, Jacinthe Gagnon, Louis A. Cuccia, John A. Capobianco, Chem. Mater., 2007, 19, 3358
32. Wenlu Ren, Gan Tian, Shan Jian, Zhanjun Gu, Liangjun Zhou, Liang Yan, Shan Jin, Wenyan Yin, Yuliang Zhao, RSC Advances, 2012, 2, 7037
33. S.H. Bo, J. Hu,Z. Chen ,Q. Wang,G.M. Xu, X.H. Liu,Z. Zhen, Appl. Phys. B, 2009, 97, 665
34. Fiorenzo Vetrone, Rafik Naccache, Venkataramanan Mahalingam, Christopher G. Morgan, John A. Capobianco, Adv. Funct. Mater., 2009, 19, 2924

35. Daqin Chen, Yunlong Yu, Feng Huang, Hang Lin, Ping Huang, Anping Yang, Zhaoxing Wang, Yuansheng Wang, J. Mater. Chem., 2012, 22, 2632
36. Dongmei Yang, Chunxia Li, Guogang Li, Mengmeng Shang, Xiaojiao Kang, Jun Lin, J. Mater. Chem., 2011, 21, 5923
37. Lei Lei, Daqin Chen, Wenjuan Zhu, Ju Xu, Yuansheng Wang, Chemistry–An Asian Journal, 2014, 9(10): 2765.
38. Wenjuan Zhu, Daqin Chen, Lei Lei, Ju Xua, Yuansheng Wang, Nanoscale, 2014, 6(18): 10500.
39. Dongmei Yang, Yunlu Dai, Jianhua Liu, Ying Zhou, Yinyin Chen, Chunxia Li, Ping'an Ma, Jun Lin, Biomaterials, 2014, 35, 2011
40. Xuesong Zhai, Shusen Liu, Xinyang Liu, Fei Wang, Daming Zhang, Guanshi Qin, Weiping Qin, J. Mater. Chem. C, 2013, 1, 1525
41. Daqin Chen, Ping Huang, Dalton Trans., 2014, 43, 11299
42. Ji-Wei Shen, Jianing Wang, Deling Kong, Xiu-Ping Yan, RSC Adv., 2014, 4, 5088
43. Noah J. J. Johnson, Andreas Korinek, Cunhai Dong, Frank C. J. M. van Veggel, J. Am. Chem. Soc. 2012, 134, 11068
44. Fan Zhang, Renchao Che, Xiaomin Li, Chi Yao, Jianping Yang, Dengke Shen, Pan Hu, Wei Li, Dongyuan Zhao, Nano Lett., 2012, 12, 2852
45. Xiaomin Li, Dengke Shen, Jianping Yang, Chi Yao, Renchao Che, Fan Zhang, Dongyuan Zhao, Chem. Mater., 2013, 25, 106
46. Xiaomin Li, Rui Wang, Fan Zhang, Dongyuan Zhao, Nano Lett., 2014, 14, 3634
47. M. Wang, C. C. Mi, W. X. Wang, C. H. Liu, Y. F. Wu, Z. R. Xu, C. B. Mao, S. K. Xu, Acs Nano, 2009, 3, 1580.
48. Peizhi Yang, Peizhen Deng, Zhiwen Yin, Journal of Luminescence 2002, 97, 51
49. D. S. Sumida, Optics Lrtters, 1994, 17, 1343